Quantitative Assessment of Changes in Muscle Contractility Due to Fatigue During NMES: An Ultrasound Imaging Approach

Zhiyu Sheng, Nitin Sharma and Kang Kim

Abstract—Objective: This paper investigates an ultrasound imaging-based non-invasive methodology to quantitatively assess changes in muscle contractility due to the fatigue induced by neuromuscular electrical stimulation (NMES). Methods: Knee extension experiments on human participants were conducted to record synchronized isometric knee force data and ultrasound images of the electrically stimulated quadriceps muscle. The data was first collected in a pre-fatigue stage and then in a post-fatigue stage. Ultrasound images were processed using a contraction rate adaptive speckle tracking algorithm. A two dimensional strain measure field was constructed based on the muscle displacement tracking results to quantify muscle contractility. Results: Analysis of the strain images showed that, between the pre-fatigue and post-fatigue stages, there were a reduction in the strain peaks, a change in the strain peak distribution, and a decrease in an area occupied by the large positive strain. Conclusion: The results indicate changes in muscle contractility due to the NMESinduced muscle fatigue. Significance: Ultrasound imaging with the proposed methodology is a promising tool for a direct NMES-induced fatigue assessment and facilitates new strategies to alleviate the effects of the NMES-induced fatigue.

Index Terms—Ultrasound imaging, neuromuscular electrical stimulation (NMES), muscle fatigue

I. INTRODUCTION

Neuromuscular electrical stimulation (NMES) is defined as an external application of a sequence of electrical pulses that elicit skeletal muscle contractions. Applications of NMES include interventions to restore lost limb functions [1], [2], muscle training [3], rehabilitation and therapeutic applications [4], [5], as well as a research tool for *in vivo* assessment of

Manuscript submitted August 21, 2018; revised February 18, 2019; revised May 3, 2019; accepted May 30, 2019. Copyright (c) 2017 IEEE. Personal use of this material is permitted. However, permission to use this material for any other purposes must be obtained from the IEEE by sending an email to pubs-permissions@ieee.org. This work is supported by NSF award number: 1646009. Any opinions, findings and conclusions or recommendations expressed in this material are those of the authors and do not necessarily reflect the views of NSF. (Corresponding authors: Nitin Sharma and Kang Kim.)

Zhiyu Sheng is with the Department of Mechanical Engineering and Materials Science, University of Pittsburgh School of Engineering, Pittsburgh, PA, USA. e-mail: zhs41@pitt.edu. Nitin Sharma and Kang Kim are with the Department of Mechanical Engineering and Materials Science and with the Department of Bioengineering, University of Pittsburgh School of Engineering, Pittsburgh, PA, USA. e-mail: nis62@pitt.edu, kangkim@upmc.edu. Nitin Sharma is also with the Clinical and Translational Science Institute at the University of Pittsburgh, Pittsburgh, PA, USA. Kang Kim is also with the Center for Ultrasound Molecular Imaging and Therapeutics, Department of Medicine and Heart and Vascular Institute, University of Pittsburgh School of Medicine and University of Pittsburgh Medical Center, Pittsburgh, PA, USA. Kang Kim is also with the McGowan Institute for Regenerative Medicine, University of Pittsburgh and University of Pittsburgh Medical Center, Pittsburgh, PA, USA.

neuromuscular function [6]. NMES when used to restore a lost limb function is also known as functional electrical stimulation (FES). NMES or FES has been successfully demonstrated to activate paralyzed or paretic muscles that in turn help restore limb functions (e.g., standing, walking, upper limb functions such as grasp and reaching) of persons with stroke, hemiplegia, paraplegia and other neurological disorders [7]. Design and control of FES is still a very active research area as evident from the following cited literature [8]–[18].

It is commonly noted that during NMES or FES control the rapid onset of muscle fatigue quickly deteriorates the force generation capability of the muscle, which causes loss of control effectiveness. This NMES-induced decreased force can be referred to as a localized muscle fatigue [19] due to a decrease in muscle contractility. Unlike volitional muscle contractions, the fatigue during NMES onsets quickly because the artificially recruited muscles do not follow the Henneman's size principle [20]. NMES synchronously recruits motor units in a non-selective, spatially fixed manner [21], and thus accelerates the onset of localized muscle fatigue and significantly limits its efficiency and operation time. Strategies for resolving this problem aim at postponing or inhibiting the progress of fatigue by specifically designing optimal stimulation patterns [22], [23], using asynchronous stimulation [18], [24], and reducing the stimulation duty cycle by sharing load or effort with a powered exoskeleton or passive orthosis [25]–[29]. These stimulation techniques work without a direct feedback of fatigue information or indirectly assess the propagation of the NMES-induced fatigue via a mathematical model [30]-[34].

Compared with the model-based assessment of muscle fatigue, we believe that directly measuring fatigue development can help design new stimulation protocols and address the fatigue issue effectively. This can potentially make the use of NMES/FES more clinically viable. Efforts in measuring fatigue include but are not limited to tetanic force measurement [35], electromyography (EMG), surface electromyography (sEMG) [36]–[42], mechanomyography (MMG) [43]– [45], near-infrared spectroscopy (NIRS) [43], [46] and phosphorus nuclear magnetic resonance (NMR) [47]. A reduced tetanic force is directly related to fatigue. However, measuring the limb joint torque is a non-trivial problem during dynamic limb movements. Besides, it is difficult to investigate fatigue of an individual muscle group in a limb joint that has multiple spanning muscles. sEMG with appropriate frequency or time domain analysis is currently the most established noninvasive approach to assess muscle fatigue. There are howeve limitations of sEMG-based fatigue assessment because th recorded signals are sensitive to electrode placement and caalso be influenced by some uncontrolled factors, for example interference from electrical stimulation [48], cross talk amon myoelectric signals from neighboring muscles [39]. Moreover sEMG is usually limited to muscles positioned directly below the skin [39]. MMG is regarded as a mechanical counterpar of EMG. A recent review [45] summarized the current chal lenges of using MMG to assess muscle functions and pointe out that this sensor modality needs further exploration an improvement, especially in experimental studies and clinica practice. NIRS and NMR reveal physiological mechanisms of muscle fatigue but in general these approaches are not easilimplementable in real-time for NMES/FES applications, wher wearability of sensing modalities is also an accounting factor

Recently, ultrasound imaging techniques have been proposed to study neuromuscular systems, prosthesis and muscl contraction and fatigue [49]–[55]. The studies demonstrate ultrasound imaging as a non-invasive, real time implementabl tool that can provide a wealth of information of a targete muscle irrespective of its depth. More importantly, ultrasoun imaging allows direct visualization of the stimulated muscle Due to its relatively high spatial and temporal resolution, 2-dimensional (2D) anatomical image of a region of interes (ROI) can be obtained and further processed to provide comprehensive information of muscle contractions.

To investigate muscle fatigue, it is necessary to determin an appropriate measure from the ultrasound images to characterize the muscle contractility change and thus capture the fatigue effect. In [55], a muscle thickness change was extracted from the cross-sectional ultrasound images to characterize an exercise-induced fatigue in the right biceps brachii muscle. In [54], elastic and viscoelastic like modifications in the 3rd flexor digitorum superficialis muscle after a fatigue exercise were captured by ultrasound strain imaging. Vøllestad in [35] argued that an appropriate and reliable measure for quantifying muscle fatigue should reflect the force generating capacity. When generating force, according to the cross bridge and sliding filament model [56]-[58], microscopic muscle contraction behavior cumulatively results in a macroscopic muscle deformation. Therefore a strain signal that quantifies the muscle deformation is an appropriate measure of the muscle fatigue. The feasibility of constructing a strain measure from ultrasound images has been explored in strain imaging technologies; e.g., the experiment on a controlled rabbit heart [59], in vivo breast tumor detection [60], tendon tissue motion and strain assessment [61], and exercised-induced fatigue assessment [54].

Compared with [54] and [55], an NMES-induced muscle fatigue is studied in this paper. We perform isometric knee extensions by stimulating the quadriceps muscle of human participants. Experiments were first conducted when the muscle was not fatigued, which were followed by a fatiguing protocol to fatigue the muscle. Experiments were then immediately repeated in the post-fatigue stage. Force data and ultrasound images were synchronously recorded. A strain measure, derived from the ultrasound images, was constructed using an

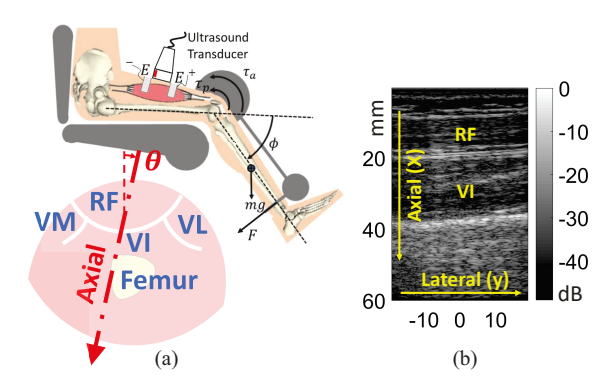


Figure 1. (a) A sketch of the stimulated isometric knee extension experiment using ultrasound imaging. Stimulation is sent through the proximal (negative) and distal (positive) electrode pads (E) to stimulate the quadriceps and produce the joint torque τ_a . The shank is attached to the rigidly fixed load cell with the normal force F so that the knee angle is constrained to a fixed angle around $\phi=75^\circ$. mg represents the gravitational force of the shank while τ_p represents the passive torque introduced by the ligament or tendon elements. The ultrasound transducer is placed along the muscle fiber with the left side (marked by the red bar) corresponding to the proximal side. The axial direction of the best imaging plane to visualize the most noticeable deformation is illustrated by a sketch of the cross-sectional quadriceps anatomy. A positive angle θ is adjustable among all the 4 subjects. (b) A longitudinal B-Mode ultrasound image showing the ROI and the coordinate system in the imaging plane.

ultrasound speckle tracking algorithm [62]. Compared with the methodology described in [54], a contraction rate adaptive scheme was introduced in this paper to deal with challenges associated with the quadriceps muscle that has a large and fast deformation, as well as a non-uniform contraction rate. A comprehensive analysis of the strain measure was performed to profile the changes in muscle contractility and the NMES-induced muscle fatigue.

II. METHOD

A. Strain Measure

During a muscle contraction, microscopic muscle behavior results in a macroscopic muscle deformation that generates force. In continuum mechanics, the deformation can be described by a deformation gradient tensor, \mathbf{F} ,

$$\mathbf{F} = \mathbf{R}\mathbf{U},\tag{1}$$

where ${\bf R}$ is a proper orthogonal tensor describing rotation while ${\bf U}$ is the right stretch tensor. With the assumption that the deformation is limited within the ultrasound imaging plane, ${\bf F}$, ${\bf R}$ and ${\bf U}$ are each represented by 2×2 matrix arrays. It is further assumed that during the whole process of contraction, the principal axes of ${\bf U}$ remain close to the axial and lateral directions of the ultrasound image coordinate system shown in Fig. 1b. Therefore, ${\bf R}$ can be taken as the identity matrix ${\bf I}$ and approximately,

$$\mathbf{F} = \mathbf{U} = \begin{bmatrix} \lambda_1 & 0 \\ 0 & \lambda_2 \end{bmatrix}, \tag{2}$$

where λ_1 , λ_2 are principal stretches along axial and lateral directions, respectively. As a result, in this study, after applying

the coordinate system specified in Fig. 1b, strain measures, ε_1 and ε_2 ,

$$\varepsilon_1(x,y) = \lambda_1(x,y) - 1, \ \varepsilon_2(x,y) = \lambda_2(x,y) - 1,$$
 (3)

reflect the force producing deformation of the quadriceps muscle activated by NMES at the position: (x,y).

Note that the quadriceps muscle as a soft tissue undergoes a large deformation. In finite strain theory a more commonly used strain measure is the Green-Lagrangian strain tensor $\mathbf{E} = \frac{1}{2} \left(\mathbf{F}^T \mathbf{F} - \mathbf{I} \right)$. However, as claimed in [59], by quantifying a fractional change of the localized element length, ε_1 , ε_2 , which are directly derived from the principal stretches, λ_1 , λ_2 , are more intuitive to characterize the muscle contractility.

It should also be noted that the strain measure can be further simplified by looking at only one of ε_1 and ε_2 due to an additional assumption of incompressibility of the skeletal muscle [63]. This is governed by a constraint equation of the volumetric measure $\det\left(\mathbf{F}(\varepsilon_1,\varepsilon_2)\right)$, where $\det\left(\cdot\right)$ denotes the determinant of (\cdot) [64]. Therefore, the resultant deterministic relationship between ε_1 and ε_2 , together with all the aforementioned assumptions, indicates that the scalar field $\varepsilon_1(x,y)$ (or $\varepsilon_2(x,y)$) can fully characterize the muscle contractility in the selected ultrasound scanning plane.

B. Contraction Rate Adaptive Speckle Tracking

To construct the strain measure from ultrasound images, a muscle contraction rate adaptive speckle tracking algorithm is applied. According to [62], a general 2D normalized cross correlation based speckle tracking algorithm for displacement estimation at a spatial position (x,y) between frame number m and n is expressed as,

$$\vec{d}_{m,n}(x,y) = (u(x,y), v(x,y))$$

$$= \arg\max_{u,v} \{\gamma(u,v)\}, \qquad (4)$$

where γ is the normalized correlation coefficient given as

$$\gamma(u,v) = \frac{\sum\limits_{K_{x,y}} (f_m(a,b) - \bar{f}_m) (f_n(a+u,b+v) - \bar{f}_{n,u,v})}{\sqrt{\sum\limits_{K_{x,y}} (f_m(a,b) - \bar{f}_m)^2 \sum\limits_{K_{x,y}} (f_n(a+u,b+v) - \bar{f}_{n,u,v})^2}},$$

$$-\frac{W_u}{2} \le u \le \frac{W_u}{2}, -\frac{W_v}{2} \le v \le \frac{W_v}{2}.$$
(5)

All the coordinates are in mm. In (5), f_m and f_n are the magnitude of the envelope extracted from beamformed ultrasound echo signals of the image frame number m and n, respectively. $(a,b) \in K_{x,y}$, where $K_{x,y}$ is the rectangular kernel centered at the position (x,y) with the size chosen as $25\Delta_x \times 11\Delta_y$. In this study the image precisions in the axial and lateral directions are $\Delta_x = 0.0385$ mm/pixel, based on the ultrasound signal sampling frequency of 20 MHz, and $\Delta_y = 0.3$ mm/pixel, based on the element pitch of the ultrasound array transducer, respectively. \bar{f}_m , $\bar{f}_{n,u,v}$ are mean values of $f_m(a,b)$ and $f_n(a+u,b+v)$, respectively, and are computed using all the data inside the kernel $K_{x,y}$. W_u , W_v form a $W_u \times W_v$ rectangular search window and are specifically set as $W_u = 26\Delta_x$, $W_v = 6\Delta_y$, by approximating the maximum range of the motion to eliminate any potential

peak hopping, as well as to minimize the computation effort. Because of pixel-based digitizing, the true maximum value in (4) usually refers to a subsample. Therefore, to achieve more accurate tracking results, the images inside the kernel and the search window are upsampled with a factor of 10 via a 2D cubic spine interpolation (not-a-knot end conditions). Multiple $\gamma(u,v)$ values close to the maximum are selected for curve fitting [65] to identify the true peak of the correlation coefficient. As a result, frame to frame displacement field $\vec{d}_{m,n}(x,y)$ can be obtained and associated with a more accurate peak of $\gamma(u,v)$. A cumulative displacement at every spatial positions with respect to the first image frame denoted by, $\vec{s}(x_0,y_0)=(s_x(x_0,y_0),s_y(x_0,y_0))$, can be computed by recurrently summing consecutive frame to frame tracking results, as

$$(x_i, y_i) = (x_{i-1}, y_{i-1}) + \vec{d}_{i-1,i}(x_{i-1}, y_{i-1}),$$
 (6)

$$\vec{s}(x_0, y_0) = (x_{N-1}, y_{N-1}) - (x_0, y_0), \tag{7}$$

where i=1...N-1 and (x_0,y_0) is the given position in the first frame (the reference), if there are in total N collected image frames and N-1 frame to frame tracking results.

Because there is a limited a priori knowledge about the accurate instantaneous tissue velocity during the entire muscle contraction process, a high frame rate (> 1.5 kHz) is preferred when imaging the quadriceps muscle. This ensures quasistatic speckle tracking and minimizes a decorrelation even in the presence of a very fast muscle movement. However, during time intervals where the images indicate relatively slow motion, consecutive frame to frame tracking is unnecessary and it only accumulates noise when computing the cumulative displacement in (6). Therefore, in our implementation, an adaptive scheme is introduced by constructing a subsequence $\{f_{j_k}\}, k = 0...M - 1$ from the original image sequence $\{f_i\},$ i = 0...N - 1, such that $j_0 = 0$, $j_{M-1} = N - 1$. Selection of the frame number j_k adapts to an approximate muscle velocity. This is achieved by observing the frame to frame variation of the speckle patterns on B-Mode images. In the future, the adaptation and frame selection will be achieved via a convergent optimization scheme. As a result, frame to frame displacement estimation is computed as $\vec{d}_{j_k,j_{k+1}}$ using (4), only among the selected j_k th frames. The cumulative displacement field $\vec{s} = (s_x, s_y)$ with respect to the first frame can be obtained by (6) and (7).

Finally, according to (3), in the coordinate system shown in Fig. 1b, the defined strain measure is equivalent to

$$\varepsilon_1(x,y) = \frac{\partial s_x}{\partial x}, \ \varepsilon_2(x,y) = \frac{\partial s_y}{\partial y},$$
 (8)

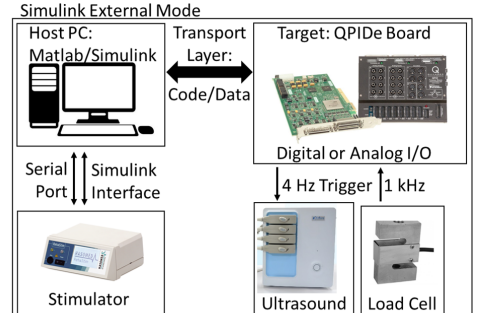
and can be obtained by applying a differentiation filter. In this study, a Savitzky-Golay filter was applied on the estimated cumulative displacement field. As previously mentioned, either one of ε_1 and ε_2 can fully characterize muscle contractility. ε_1 , obtained by taking gradient of $s_x(x,y)$ along the axial direction, is preferred in a sense that a higher precision ($\Delta_x=0.0385$ mm/pixel) along the axial direction results in better smoothing performance for a differentiation filter with a fixed kernel length.

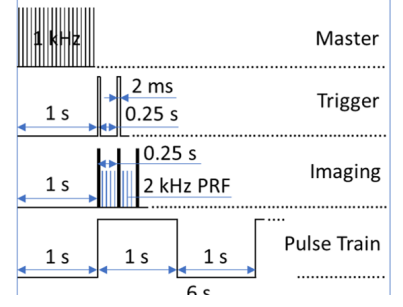
C. Apparatus and Experiment

The experiments aim to investigate the response of the quadriceps muscle to NMES via ultrasound imaging and demonstrate that the defined strain measure constructed from images in the scanned ROI can successfully capture the effect of the NMES-induced muscle fatigue. Data analysis of the strain measure including the maximum value and the spatial distribution of the scalar field ε_1 , as well as the area of large positive ε_1 , is conducted and compared between pre and post fatigue stages. The post-fatigue stage is attained by stimulating the quadriceps muscle as per a fatiguing protocol that induces a reduction in the knee joint torque. 4 able bodied subjects (S1, S2, S3, S4) including 3 male and 1 female in a range of 22 to 27 years old consented to participate in the experiments. The procedures and protocols were approved by the Institutional Review Board (IRB) of the University of Pittsburgh. The experimental setup and procedures are described as follows.

- 1) Locating Imaging ROI: As described in Fig. 1, the ultrasound transducer is placed on the thigh, approximately along the muscle fiber direction, to obtain longitudinal quadriceps images. On the image, as in Fig. 1b, the proximal side of the thigh is on the left while the distal side is on the right. Due to the fact that the image data collected will depend on ultrasound transducer placement, it is necessary to locate and fix the accurate ROI. This was done by locating the targeted muscle and testing its response to stimulations via the ultrasound image. The transducer placement was adjusted accordingly. We do not precisely distinguish the contributions of muscle contraction from rectus femoris (RF), vastus lateralis (VL), vastus medialis (VM) and vastus intermedius (VI) due to NMES. The best imaging plane, as shown in Fig. 1a, is chosen to visualize the most noticeable deformation of the entire quadriceps muscle and meanwhile minimize outof-plane motions. This provides images with stronger and more stable signals. Once the placement of the transducer was finalized, the position and the orientation were kept by a commercial transducer holder (with single-axis positioning stage, Quipu, Italy) during the whole experiment.
- 2) Data Collection in Pre-fatigue and Post-fatigue Stages: The experimental setup is illustrated in Fig. 2a, where the human participant is seated on a leg extension machine. An isometric knee extension task was conducted by stimulating the quadriceps while fully constraining the knee joint angle with a load cell (LC101-150, OMEGA Engineering, USA), which was fixed rigidly and attached normally to the front of the shank. As the stimulated leg tends to move against the constraint, the load cell records the force. As shown in Fig. 1a, according to the balance equation of F, τ_a , mg and τ_p , load cell data reflects the force generated by the quadriceps muscle contraction at the knee joint. Stimulation pulse trains were sent from a stimulator (Rehastim 1, HASOMED GmbH, Germany) to recruit the quadriceps muscle through two large electrodes (10×7.5 cm) placed along the thigh. The proximal one was placed towards the lateral side while the distal was placed around the midline and slightly to the medial side to include the motor point of the quadriceps muscle [42]. A clinical linear transducer (L7.5SC Prodigy Probe, S-Sharp,

- Taiwan) connected to the ultrasound imaging system (Prodigy, S-Sharp, Taiwan) was used to image the contraction of the quadriceps muscle. The force and ultrasound image data was first collected in the pre-fatigue stage. This was followed by a fatiguing stimulation protocol to induce fatigue. The force and image data was then collected in the post-fatigue stage using the same protocol as in the pre-fatigue stage. In both stages, three stimulation pulse trains were used after the 1 s initial delay. Duration of each train was set to 1 s and there was a 1 s rest period between the consecutive trains. Waveform parameters of the stimulation were chosen as: amplitude of 26 mA, pulse frequency of 35 Hz and pulse width of 300 µs. The stimulation parameters are within a typical range reported in various NMES controlled leg extension studies [17], [28], [66]. The constant amplitude, which is in a range reported in [66], was chosen so that significant muscle contractions and the related knee extensions were observed, while also considering the comfort-level of the participants to the stimulation amplitude. The pulse frequency and the pulse width were selected within a range that is optimal and produces predictable force [66]. Ultrasound plane wave imaging with parameters of 5 MHz center frequency, 20 MHz sampling frequency and 2000 frames per second (FPS = 2 kHz) was used to scan the ROI. A 10 min break was provided after preliminary stimulation of the quadriceps muscle to ensure that the experiment starts in the pre-fatigue stage. The preliminary tests were performed to find the best ultrasound transducer placement. However, no rest was provided between the end of the fatiguing protocol and the post-fatigue stage.
- 3) Fatiguing Protocol: The fatiguing protocol is designed to be more intense so that the quadriceps muscle can be guaranteed to be in a fatigued status after being stimulated for a certain time period. However, the parameter of NMES should still operate within the suggested range of a knee extension [17], [28], [66] and should not compromise the comfort-level of the participants. As a result, each stimulation pulse train's duration was increased to 1.5 s. The stimulation trains lasted 80 s in total duration. The rest period between the trains was decreased to 0.5 s. The following stimulation parameters were used: 28 mA amplitude, 35 Hz pulse frequency and 300 µs pulse width. Due to the fatiguing protocol the muscle force of subject S3 decreased from approximately 40 N to 15 N. The decay in the force is shown in Fig. 3b. The reduction in the force was consistently observed among all the subjects.
- 4) Data Synchronization: Data synchronization needs to be ensured so that stimulation pulse trains, sampling frequency of force measurement, ultrasound imaging frame rate, as well as the time window of data collection can be set according to the unique time base. To achieve this, a real time system is implemented in Matlab/Simulink (MathWorks, USA) as shown in Fig. 2b. During typical data collection process as in Fig. 2c, the main Simulink program runs on the real time target (QPIDe Board, Quanser, Canada) with a time base of 1 kHz, which is governed by an internal hardware clock (24-bit counter) on the board. With respect to this time base, a 4 Hz pulse train with 0.8 % duty cycle is sent through the digital output channel, as a trigger in signal, to the S-sharp ultrasound imaging system, while the load cell sends force measurement data through the





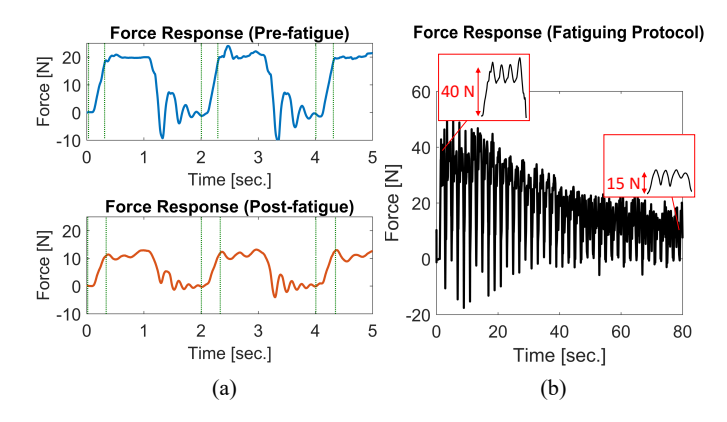


Figure 3. (a) The recorded force data from pre (top) and post (bottom) fatigue stages of subject S3. Among the three contraction cycles, the rising periods marked by the dotted lines were extracted and segmented for further analysis. (b) The fatiguing process of subject S3 governed by the force measurement from the load cell. The decay of the force from an initial level, that is around 40 N, to a steady state, that is around 15 N, indicates that the muscle is fatigued.

analog input channel at the sampling frequency of 1 kHz. To achieve 2 kHz FPS plane wave imaging, the S-sharp system is configured via sequence programming to synchronously and repeatedly fire all the 128 channels, 500 times within 0.25 s, every time a trigger in pulse from QPIDe is received. A 1 s period is intentionally left at the beginning in order to guarantee that all the devices are ready for data collection after initialization.

III. RESULTS AND DISCUSSION

A. Data Process and Segmentation

Fig. 3a shows the force response to stimulation in both pre and post fatigue stages. Under the designed experiment protocol of data collection and synchronization scheme, the recorded force curves span 5 s on the time axis after the initial 1 s time period. During each trial, there were 3 flat peaks of force response representing 3 contraction cycles, from which, the rising periods towards the maximum values were

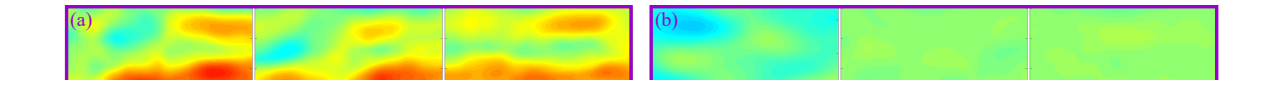
extracted, as illustrated by the dotted lines in Fig. 3a, and subtracted by the initial value of each segment. By assuming that fatigue remains the constant level within each trial but has noticeable variation after the fatiguing process as in Fig. 3b, these 3 segments together with their synchronized ultrasound images can be considered as 3 repeated measurements of an independent data set from one subject. The same process and segmentation was repeated for data of all the 4 subjects. Consequently, 12 data segments in pre-fatigue stages and 12 data segments in post-fatigue stages were obtained. The defined strain measure $\varepsilon_1(x,y)$ in (3) in each of the 24 data segments was constructed using the method introduced in Section II B with the kernel size of a Savitzky-Golay filter adjusted between 2.5 to 3.5 mm.

B. Images of Strain Peaks in Pre-fatigue and Post-fatigue Stages

The computed scalar field $\varepsilon_1(x,y)$ of the frame corresponding to the maximum force was selected from each segmented data set. These images are named as Pre-1, 2, 3 and Post-1, 2, 3 in the pre-fatigue and post-fatigue stages, respectively. They contain positive strain peaks and quantify the contractile deformation, which is a noticeable expansion along the axial direction and produces the maximum force during each muscle contraction. Sub-figures (a)-(c) of Figs. 4-7 summarize and show the comparison between pre and post fatigue stages of all of the 4 participants (S1, S2, S3, S4) in a rectangular ROI. Several facts should be noticed for discussion.

Firstly, in both pre and post fatigue stages of a subject, the pattern of the scalar field $\varepsilon_1(x,y)$ is overall consistent among Pre-1, 2, 3 and Post-1, 2, 3 images. This demonstrates the performance and robustness of the methodology to characterize stimulated muscle contraction using the defined strain measure. Relatively large deformation is more spatially distributed in the pre-fatigue stage. The deformation, however, completely disappears or concentrates in a smaller region after the fatiguing protocol. For example, in sub-figures (a)-(c) of Fig. 6, the maximum of S3 usually occurs around the location

This article



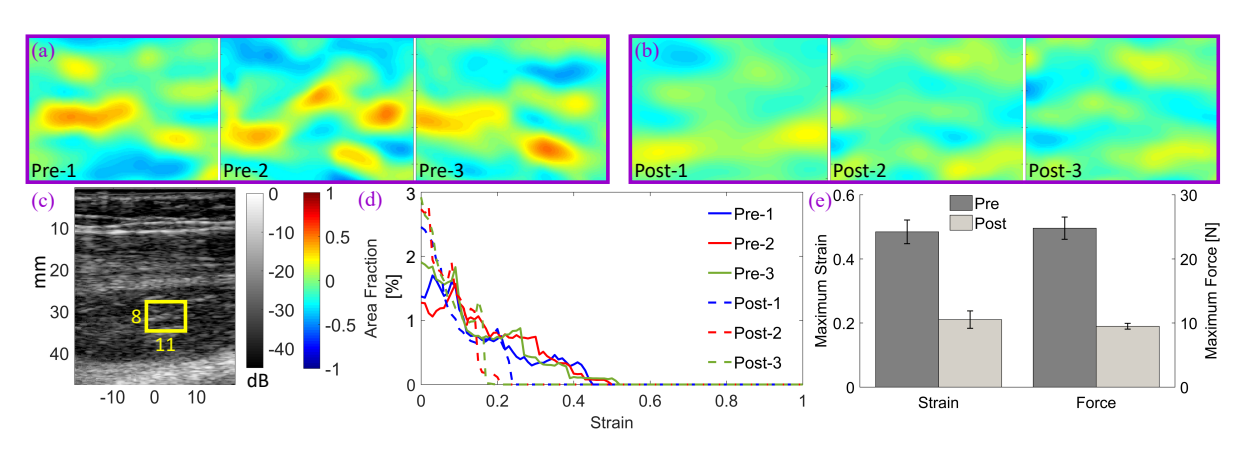


Figure 5. Comparison between pre-fatigue and post-fatigue stages of subject S2.

 $x = 29.0 \sim 33.0$ mm, $y = 2.0 \sim 10.0$ mm in the prefatigue stages and around the location $x=29.0 \sim 30.0$ mm, $y = 3.0 \sim 5.0$ mm in the post-fatigue stages. It should be noted that some specific strain patterns do not necessarily stay in the exactly same locations. For example, it is observed that in Fig. 6a, the region containing large strain values in Pre-1 image slightly shifts toward the positive direction along the axial axis, compared with the images in Pre-2 and Pre-3. In Fig. 6b, the strain peak of Post-3 image laterally locates at a position of smaller y coordinate compared with Post-1 and Post-2 images. This is attributed to multiple facts including a little but inevitable artifact movement of the ultrasound transducer, small rigid body motion of the whole ROI because of an imperfect isometric condition, other random uncontrolled noisy aspects during imaging and speckle tracking, etc. Nevertheless, the overall quality of the results is not impaired because the pattern in the selected region is still consistently discernible and comparable between pre and post fatigue stages.

Secondly, there is a noticeable reduction in the strain peaks if a one on one comparison is conducted between data sets of Pre-1, 2, 3 and Post-1, 2, 3, respectively. The peak reduction is not only captured by intuitive observation, but also implied by the following two measures. One is the overall maximum

 $\varepsilon_{1,max}$. $\varepsilon_{1,max}$ is computed by taking the median number of the 12 largest $\varepsilon_1(x,y)$ among all the pixel positions of an image. The median is used to rule out potential abnormal peaks due to data noise. The resultant $\varepsilon_{1,max}$ value during each comparison is summarized by the sub-figures (e) of Figs. 4-7. It is further discussed in Section III C. The second measure is the strain peak reduction in the same local region. For example, data of S3 has multiple spatially distributed strain peaks in the pre-fatigue stage, as shown by Fig. 6a. The maximum of $\varepsilon_1(x,y)$ in the region, $x=29.0\sim32.0$ mm, $y=3.0\sim6.0$ mm, reduces from 0.538 in Pre-1 to 0.350 in Post-1, from 0.517 in Pre-2 to 0.391 in Post-2 and from 0.706 in Pre-3 to 0.377 Post-3, respectively. Either of the two measures shows an apparent reduction in the strain peaks.

Finally, sub-figures (d) of Figs. 4-7 further quantify an additional aspect of the fatigue effect, which is, a change of the spatial distribution of the strain peaks. These histograms that represent the area fraction (%) are created by comparing sub-figures (a) of Figs. 4-7 and sub-figures (b) of Figs. 4-7. The area fraction (%) are calculated by first counting the number of pixels, whose strain values belong to consecutive 0.010-long intervals, and second dividing the counted number by the number of all the pixels on an image. The results in a range of [0.000, 1.000] are shown to depict the area fraction of

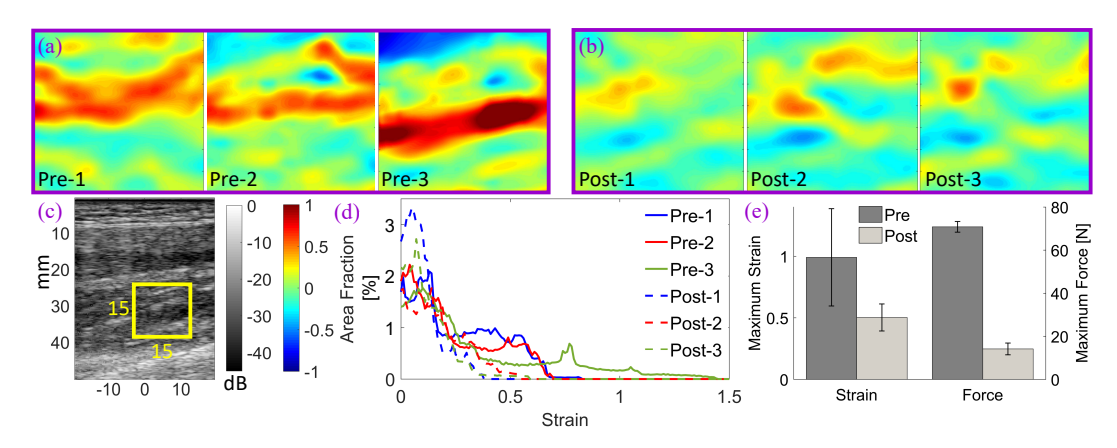


Figure 7. Comparison between pre-fatigue and post-fatigue stages of subject S4.

the positive strain values. Comparison of area fraction curves between pre and post fatigue stages indicates a change in strain distributions. The range of Fig. 7d was adjusted to [0.000, 1.500] because subject S4 had large positive strain values in the pre-fatigue stage. As a result, it is observed that in the post-fatigue stage of each participant, the area fraction consistently shows an apparent higher peak around 0 while the large positive strain values occupy much less area compared to the pre-fatigue stage. Specifically for subject S1 in Fig. 4d, the widely spread area fraction in the pre-fatgiue stage concentrates around a very sharp peak in the post-fatigue stage, whereas the field of $\varepsilon_1(x,y)$ becomes almost a uniform zero map in Fig. 4b. A quantitative way to describe this trend can be done by setting an appropriate threshold t_{ε} , and then calculating the total area fraction of $\varepsilon_1 \geq t_{\varepsilon}$. The threshold t_{ε} should be not only a number above the noise level after the whole signal processing, but also a conservative small number in order not to artificially rule out the potential small strain peaks. In this paper, $t_{\varepsilon} = 0.25$ was chosen and the calculated area fraction of $\varepsilon_1 \ge 0.25$ had a significant decrease compared between the pre and post fatigue stages, as shown by the subsequent statistical analysis.

C. Comparing Peak Reduction of the Strain Measure and Force

 $arepsilon_{1,max}$ values as introduced in Section III B are computed in each segmented data set. The corresponding maximum force

Table I THE MAXIMUM FORCE AND THE MAXIMUM STRAIN (MEAN \pm SAMPLE STANDARD DEVIATION)

		Pre	Post
S1	F_{max}	13.2 ± 0.647	2.17 ± 0.622
	$\varepsilon_{1,max}$	0.615 ± 0.0846	0.0871 ± 0.0166
S2	F_{max}	24.8 ± 1.73	9.49 ± 0.453
	$\varepsilon_{1,max}$	0.484 ± 0.0369	0.210 ± 0.0271
S 3	F_{max}	20.0 ± 1.16	12.3 ± 0.875
	$\varepsilon_{1,max}$	0.690 ± 0.113	0.373 ± 0.0171
S4	F_{max}	70.8 ± 2.49	14.1 ± 2.71
.54	$\varepsilon_{1,max}$	0.991 ± 0.395	0.502 ± 0.110

in that data set is denoted as F_{max} . Comparison of $\varepsilon_{1,max}$ and F_{max} between pre-fatigue and post-fatigue stages for each subject is summarized by sub-figures (e) of Figs. 4-7 and Tab. I. A similar trend in the peak reduction is observed for the strain and force data for each subject and the reduction is significant as shown by the subsequent statistical analysis among all the data samples of S1-S4. As a pilot study, it is premature to draw definitive on the accurate quantitative dependency between F_{max} and $\varepsilon_{1,max}$ without further investigating the transition period from non-fatigued to completely fatigued status. However, the presented results clearly demonstrate that the strain measure potentially has a correlation with the force produced during a muscle contraction. The reduction of force validates the effectiveness of the designed fatiguing protocol while the reduction of strain demonstrates the capability of as-

T , IEEE

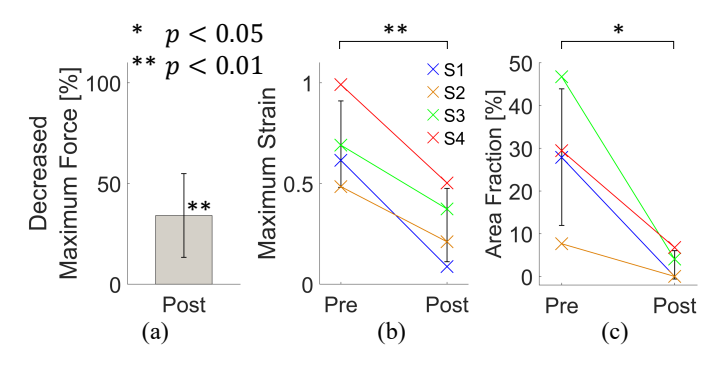


Figure 8. (a) A two-tailed one-sample t-test (p < 0.01) of the decreased maximum force, compared to 100 %. (b) A two-tailed paired t-test (p < 0.01) of the maximum strain, compared between the pre and post fatigue stages. (c) A two-tailed paired t-test (p < 0.05) of the area fraction where strain is greater than 0.25, compared between the pre and post fatigue stages.

sessing the change in muscle contractility due to the fatiguing protocol. Future research will target on modeling the whole fatiguing process by investigating variant muscle contractility during a transition period (i.e., from no-fatigued to fatigued status). It is also observed that variance of $\varepsilon_{1,max}$ is relatively large in the pre-fatigue stage while that of force is close in both pre and post fatigue stages. This is most likely due to the fact that more noisy factors and artifacts are introduced in speckle tracking and image processing when non-fatigued muscle creates deformation at a higher contraction speed.

D. Statistical Analysis

Two-tailed Student's t-tests were performed on data samples of F_{max} , $\varepsilon_{1,max}$ and the area fraction of $\varepsilon_1 \geq 0.25$, respectively. In each test, according to the experiment protocol, one independent data sample refers to each subject S_i (i = 1, 2, 3, 4) and is obtained by calculating the mean of the 3 quadriceps muscle contractions. A one-sample t-test was performed on the decreased F_{max} (%) in the post-fatigue stage with respect to the maximum force each subject can produce when he or she is not fatigued. The decreased maximum force follows a normal distribution, validated by a Shapiro-Wilk test (p = 0.45), and has a significant decrease (p < 0.01), compared to 100 %, as shown by Fig. 8a. For $\varepsilon_{1,max}$ and the area fraction of $\varepsilon_1 \geq 0.25$, respectively, 4 data samples were obtained and compared between pre and post fatigue stages through the paired t-tests. The data normality was also validated by the Shapiro-Wilk tests. The difference between pre and post fatigue stages of $\varepsilon_{1,max}$ and the area fraction, respectively, follows a normal distribution with p = 0.33 and p = 0.97, respectively. Consequently, as shown by Fig. 8b and Fig. 8c, $\varepsilon_{1,max}$ and the area fraction both have a significant decrease with p < 0.01 and p < 0.05, respectively.

The significant reduction of F_{max} validates that the used stimulation parameters of the fatiguing NMES protocol can fatigue the quadriceps muscle. In the post-fatigue stage, the decreased muscle contractility represented by a lesser deformation is further noted by the significantly reduced $\varepsilon_{1,max}$ and the area fraction above a threshold of 0.25. An explanation of the reduction of both the magnitude of the strain peaks and the area fraction is that muscle in all of the stimulated

area experienced fatigue once recruited by NMES in a temporally synchronous pattern [21]. The peaks of the scalar field, $\varepsilon_1(x,y)$, during each contraction overall decreased across the stimulated area. However, the reduction rate in different locations were not uniform possibly because muscle fibers are of different types [21] and have different responses to fatigue. In some area, strain peaks disappeared with the value close to zero when muscle in those regions hardly respond to the stimulation anymore. In other area, some obvious peaks remained with non-zero values when the muscle in those regions was believed to be more fatigue endurable. As a result, we observed that both the peak values and the area fraction of the strain decreased. Results of the performed t-test support the observations and discussions in Section III B and Section III C.

E. Future Studies and Feedback of Fatigue Information in a Hybrid Neuroprosthesis

In our previous work [67], control strategies with switched scheme were designed to facilitate fatigue issues in a hybrid neuroprosthesis. The signal that triggers a switch event was based on a predictive fatigue model. The ultrasound imagingderived strain measures can possibly be used as triggering or control signals in the hybrid neuroprosthesis. The following ultrasound imaging-derived signals can be used to indicate fatigue: 1) crossing a threshold or limit set by the maximum value normalized by the NMES input in a strain image of an ROI and 2) crossing a threshold or limit set by the area of the strain peaks in an ROI. The area can be calculated by counting the number of pixels whose strain values normalized by the NMES input are greater than a threshold. There will be further studies on validating the effectiveness of using ultrasound imaging-derived fatigue signals in FES control or hybrid neuroprosthesis control strategies. Selections of ROIs where the strain measure is computed will be fixed for a participant user, after preliminary tests. Real time strain image processing will be achieved by preliminarily determining fixed optimal parameters or implementing online adaptive schemes. Further, a wearable ultrasound transducer will be developed and sensitivity of the results to slightly different imaging locations and orientations will be investigated.

Finally, it should be noted that all the observations and implications presented depend on the defined strain measure, whose rationale is based on all the assumptions described in Section II A. Future studies will aim at improving ultrasound speckle tracking performance by incorporating regularization and noise rejecting schemes. This will enable successfully reconstructing full elements of the tensors **F**, **R** and **U** in (1) so that the presented methodology can be applied to analysis of muscle contractility in more general scenarios, where the targeted muscle follows less or none of those aforementioned assumptions.

IV. CONCLUSION

An ultrasound imaging-based methodology to assess changes in muscle contractility due to the NMES-induced muscle fatigue was proposed and demonstrated via isometric knee extension experiments. An analysis of strain measure constructed from the ultrasound images was presented. Based on the results, it can be concluded that NMES-induced changes in muscle contractility and the fatigue effect can be quantified by an apparent reduction in the strain peaks during each stimulated contraction. A noticeable difference in strain peak distributions can be used as the second quantitative assessment of muscle contractility change. It was also shown that the area where strain peaks occur significantly decreases due to the NMES-induced fatigue.

ACKNOWLEDGMENT

This research was supported in part by the University of Pittsburgh Center for Research Computing through the resources provided.

REFERENCES

- J. Chae, L. Sheffler, and J. Knutson, "Neuromuscular electrical stimulation for motor restoration in hemiplegia," *Top. Stroke Rehabil.*, vol. 15, no. 5, pp. 412–426, 2008.
- [2] E. Marsolais and R. Kobetic, "Functional electrical stimulation for walking in paraplegia." J. Bone Joint Surg., vol. 69, no. 5, pp. 728– 733, 1987.
- [3] D. Currier and R. Mann, "Muscular strength development by electrical stimulation in healthy individuals," *Phys. Ther.*, vol. 63, no. 6, pp. 915– 921, 1983.
- [4] L. Griffin, M. Decker, J. Hwang, B. Wang, K. Kitchen, Z. Ding, and J. Ivy, "Functional electrical stimulation cycling improves body composition, metabolic and neural factors in persons with spinal cord injury," *J. Electromyogr. Kinesiol.*, vol. 19, no. 4, pp. 614–622, 2009.
- [5] B. J. Andrews and G. D. Wheeler, "Functional and therapeutic benefits of electrical stimulation after spinal injury." *Curr. Opin. Neurol.*, vol. 8, no. 6, pp. 461–466, 1995.
- [6] N. A. Maffiuletti, "Physiological and methodological considerations for the use of neuromuscular electrical stimulation," Eur. J. Appl. Physiol., vol. 110, no. 2, pp. 223–234, 2010.
- [7] P. H. Peckham and J. S. Knutson, "Functional electrical stimulation for neuromuscular applications," *Annu. Rev. Biomed. Eng.*, vol. 7, pp. 327– 360, 2005.
- [8] J. J. Abbas and H. J. Chizeck, "Feedback control of coronal plane hip angle in paraplegic subjects using functional neuromuscular stimulation," *IEEE Trans. Biomed. Eng.*, vol. 38, no. 7, pp. 687–698, 1991.
- [9] C. L. Lynch and M. R. Popovic, "Functional electrical stimulation," IEEE Control Syst., vol. 28, no. 2, pp. 40–50, 2008.
- [10] A. Ajoudani and A. Erfanian, "A neuro-sliding-mode control with adaptive modeling of uncertainty for control of movement in paralyzed limbs using functional electrical stimulation," *IEEE Trans. Biomed. Eng.*, vol. 56, no. 7, pp. 1771–1780, 2009.
- [11] C. Freeman, A.-M. Hughes, J. Burridge, P. Chappell, P. Lewin, and E. Rogers, "Iterative learning control of FES applied to the upper extremity for rehabilitation," *Control Eng. Pract.*, vol. 17, no. 3, pp. 368–381, 2009.
- [12] N. Sharma, K. Stegath, C. M. Gregory, and W. E. Dixon, "Nonlinear neuromuscular electrical stimulation tracking control of a human limb," *IEEE Trans. Neural Syst. Rehabil. Eng.*, vol. 17, no. 6, pp. 576–584, 2009.
- [13] N. Sharma, C. Gregory, and W. E. Dixon, "Predictor-based compensation for electromechanical delay during neuromuscular electrical stimulation," *IEEE Trans. Neural Syst. Rehabil. Eng.*, vol. 19, no. 6, pp. 601– 611, 2011.
- [14] N. Sharma, C. M. Gregory, M. Johnson, and W. E. Dixon, "Closed-loop neural network-based NMES control for human limb tracking," *IEEE Trans. Control Syst. Technol.*, vol. 20, no. 3, pp. 712–725, 2012.
- [15] E. Schearer, Y.-W. Liao, E. Perreault, M. Tresch, W. Memberg, R. Kirsch, and K. Lynch, "Multi-muscle FES force control of the human arm for arbitrary goals," *IEEE Trans. Neural Syst. Rehabil. Eng.*, vol. 22, no. 3, pp. 654–663, 2014.
- [16] N. Alibeji, N. Kirsch, S. Farrokhi, and N. Sharma, "Further results on predictor-based control of neuromuscular electrical stimulation," *IEEE Trans. Neural Syst. Rehabil. Eng.*, vol. 23, no. 6, pp. 1095–1105, 2015.

- [17] N. Alibeji, N. Kirsch, B. E. Dicianno, and N. Sharma, "A modified dynamic surface controller for delayed neuromuscular electrical stimulation," *IEEE/ASME Trans. Mechatronics*, vol. 22, no. 4, pp. 1755–1764, 2017.
- [18] R. J. Downey, T. H. Cheng, M. J. Bellman, and W. E. Dixon, "Switched tracking control of the lower limb during asynchronous neuromuscular electrical stimulation: theory and experiments," *IEEE Trans. Cybern.*, vol. 47, no. 5, pp. 1251–1262, 2017.
- [19] D. B. Chaffin, "Localized muscle fatigue-definition and measurement," J. Occup. Environ. Med., vol. 15, no. 4, pp. 346–354, 1973.
- [20] E. Henneman, G. Somjen, and D. O. Carpenter, "Excitability and inhibitibility of motoneurons of different sizes," *J. Neurophysiol.*, vol. 28, no. 3, pp. 599–620, 1965.
- [21] C. S. Bickel, C. M. Gregory, and J. C. Dean, "Motor unit recruitment during neuromuscular electrical stimulation: a critical appraisal," *Eur. J. Appl. Physiol.*, vol. 111, no. 10, pp. 2399–2407, 2011.
- [22] B. D. Doll, N. A. Kirsch, X. Bao, B. E. Dicianno, and N. Sharma, "Dynamic optimization of stimulation frequency to reduce isometric muscle fatigue using a modified hill-huxley model," *Muscle Nerve*, vol. 57, no. 4, pp. 634–641, 2018.
- [23] Z. Z. Karu, W. K. Durfee, and A. M. Barzilai, "Reducing muscle fatigue in fes applications by stimulating with n-let pulse trains," *IEEE Trans. Biomed. Eng.*, vol. 42, no. 8, pp. 809–817, 1995.
- [24] D. G. Sayenko, R. Nguyen, M. R. Popovic, and K. Masani, "Reducing muscle fatigue during transcutaneous neuromuscular electrical stimulation by spatially and sequentially distributing electrical stimulation sources," *Eur. J. Appl. Physiol.*, vol. 114, no. 4, pp. 793–804, 2014.
- [25] M. Goldfarb, K. Korkowski, B. Harrold, and W. Durfee, "Preliminary evaluation of a controlled-brake orthosis for FES-aided gait," *IEEE Trans. Neural Syst. Rehabil. Eng.*, vol. 11, no. 3, pp. 241–248, 2003.
- [26] C. To, R. Kobetic, J. Schnellenberger, M. Audu, and R. Triolo, "Design of a variable constraint hip mechanism for a hybrid neuroprosthesis to restore gait after spinal cord injury," *IEEE/ASME Trans. Mechatronics*, vol. 13, no. 2, pp. 197–205, 2008.
- [27] N. Alibeji, N. Kirsch, and N. Sharma, "An adaptive low-dimensional control to compensate for actuator redundancy and fes-induced muscle fatigue in a hybrid neuroprosthesis," *Control Eng. Pract.*, vol. 59, pp. 204–219, 2017.
- [28] N. A. Kirsch, X. Bao, N. A. Alibeji, B. E. Dicianno, and N. Sharma, "Model-based dynamic control allocation in a hybrid neuroprosthesis," *IEEE Trans. Neural Syst. Rehabil. Eng.*, vol. 26, no. 1, pp. 224–232, 2018.
- [29] K. H. Ha, S. A. Murray, and M. Goldfarb, "An approach for the cooperative control of FES with a powered exoskeleton during level walking for persons with paraplegia," *IEEE Trans. Neural Syst. Rehabil. Eng.*, vol. 24, no. 4, pp. 455–466, 2016.
- [30] J. Ding, A. Wexler, and S. Binder-Macleod, "A predictive fatigue model. I. predicting the effect of stimulation frequency and pattern on fatigue," *IEEE Trans. Rehabil. Eng.*, vol. 10, no. 1, pp. 48–58, 2002.
- [31] ——, "A predictive fatigue model. II. predicting the effect of resting times on fatigue," *IEEE Trans. Rehabil. Eng.*, vol. 10, no. 1, pp. 59–67, 2002.
- [32] R. Riener, J. Quintern, and G. Schmidt, "Biomechanical model of the human knee evaluated by neuromuscular stimulation," *J. Biomech.*, vol. 29, pp. 1157–1167, 1996.
- [33] L. A. Frey-Law, J. M. Looft, and J. Heitsman, "A three-compartment muscle fatigue model accurately predicts joint-specific maximum endurance times for sustained isometric tasks," *J. Biomech.*, vol. 45, no. 10, pp. 1803–1808, 2012.
- [34] J. Z. Liu, R. W. Brown, and G. H. Yue, "A dynamical model of muscle activation, fatigue, and recovery," *Biophys. J.*, vol. 82, no. 5, pp. 2344– 2359, 2002.
- [35] N. K. Vøllestad, "Measurement of human muscle fatigue," J. Neurosci. Methods, vol. 74, no. 2, pp. 219–227, 1997.
- [36] G. C. Knowlton, R. L. Bennett, and R. McClure, "Electromyography of fatigue." Arch. Phys. Med. Rehabil., vol. 32, no. 10, pp. 648–652, 1951.
- [37] T. Sadoyama and H. Miyano, "Frequency analysis of surface EMG to evaluation of muscle fatigue," Eur. J. Appl. Physiol. Occup. Physiol., vol. 47, no. 3, pp. 239–246, 1981.
- [38] N. C. Chesler and W. K. Durfee, "Surface EMG as a fatigue indicator during FES-induced isometric muscle contractions," *J. Electromyogr. Kinesiol.*, vol. 7, no. 1, pp. 27–38, 1997.
- [39] M. Cifrek, V. Medved, S. Tonković, and S. Ostojić, "Surface EMG based muscle fatigue evaluation in biomechanics," *Clin. Biomech.*, vol. 24, no. 4, pp. 327–340, 2009.

- [40] A. Georgakis, L. K. Stergioulas, and G. Giakas, "Fatigue analysis of the surface EMG signal in isometric constant force contractions using the averaged instantaneous frequency," *IEEE Trans. Biomed. Eng.*, vol. 50, no. 2, pp. 262–265, 2003.
- [41] D. R. Rogers and D. T. MacIsaac, "EMG-based muscle fatigue assessment during dynamic contractions using principal component analysis," *J. Electromyogr. Kinesiol.*, vol. 21, no. 5, pp. 811–818, 2011.
- [42] J. Mizrahi, M. Levy, H. Ring, E. Isakov, and A. Liberson, "EMG as an indicator of fatigue in isometrically FES-activated paralyzed muscles," *IEEE Trans. Neural Syst. Rehabil. Eng.*, vol. 2, no. 2, pp. 57–65, 1994.
- [43] Y. Yoshitake, H. Ue, M. Miyazaki, and T. Moritani, "Assessment of lower-back muscle fatigue using electromyography, mechanomyography, and near-infrared spectroscopy," *Eur. J. Appl. Physiol.*, vol. 84, no. 3, pp. 174–179, 2001.
- [44] M. Shinohara and K. Søgaard, "Mechanomyography for studying force fluctuations and muscle fatigue," *Exerc. Sport Sci. Rev.*, vol. 34, no. 2, pp. 59–64, 2006.
- [45] M. O. Ibitoye, N. A. Hamzaid, J. M. Zuniga, and A. K. A. Wahab, "Mechanomyography and muscle function assessment: A review of current state and prospects," *Clin. Biomech.*, vol. 29, no. 6, pp. 691– 704, 2014.
- [46] J. Taelman, J. Vanderhaegen, M. Robijns, G. Naulaers, A. Spaepen, and S. Van Huffel, "Estimation of muscle fatigue using surface electromyography and near-infrared spectroscopy," in *Oxygen Transport to Tissue XXXII*. New York, NY: Springer, 2011, pp. 353–359.
- [47] M. J. Dawson, D. Gadian, and D. Wilkie, "Muscular fatigue investigated by phosphorus nuclear magnetic resonance," *Nature*, vol. 274, no. 5674, pp. 861–866, 1978.
- [48] F. Mandrile, D. Farina, M. Pozzo, and R. Merletti, "Stimulation artifact in surface EMG signal: effect of the stimulation waveform, detection system, and current amplitude using hybrid stimulation technique," *IEEE Trans. Neural Syst. Rehabil. Eng.*, vol. 11, no. 4, pp. 407–415, 2003.
- [49] P. Hodges, L. Pengel, R. Herbert, and S. Gandevia, "Measurement of muscle contraction with ultrasound imaging," *Muscle Nerve*, vol. 27, no. 6, pp. 682–692, 2003.
- [50] R. S. Witte, D. Dow, R. Olafsson, Y. Shi, and M. O'donnell, "High resolution ultrasound imaging of skeletal muscle dynamics and effects of fatigue," in *Proc. IEEE Ultrason. Symp.*, vol. 1, 2004, pp. 764–767.
- [51] C. Castellini, G. Passig, and E. Zarka, "Using ultrasound images of the forearm to predict finger positions," *IEEE Trans. Neural Syst. Rehabil. Eng.*, vol. 20, no. 6, pp. 788–797, 2012.
- [52] J. Li, Y. Zhou, K. Ivanov, and Y.-P. Zheng, "Estimation and visualization of longitudinal muscle motion using ultrasonography: a feasibility study," *Ultrasonics*, vol. 54, no. 3, pp. 779–788, 2014.
- [53] S. Sikdar, H. Rangwala, E. B. Eastlake, I. A. Hunt, A. J. Nelson, J. Devanathan, A. Shin, and J. J. Pancrazio, "Novel method for predicting dexterous individual finger movements by imaging muscle activity using a wearable ultrasonic system," *IEEE Trans. Neural Syst. Rehabil. Eng.*, vol. 22, no. 1, pp. 69–76, 2014.
- [54] R. S. Witte, K. Kim, B. J. Martin, and M. O'Donnell, "Effect of fatigue on muscle elasticity in the human forearm using ultrasound strain imaging," in *Proc. IEEE Int. Conf. Eng. Med. Biol. Soc.*, 2006, pp. 4490– 4493.
- [55] J. Shi, Y.-P. Zheng, X. Chen, and Q.-H. Huang, "Assessment of muscle fatigue using sonomyography: muscle thickness change detected from ultrasound images," *Med. Eng. Phys.*, vol. 29, no. 4, pp. 472–479, 2007.
- [56] H. E. Huxley, "The mechanism of muscular contraction," *Science*, vol. 164, no. 3886, pp. 1356–1365, 1969.
- [57] T. L. Hill, "Theoretical formalism for the sliding filament model of contraction of striated muscle part i," *Prog. Biophys. Mol. Biol.*, vol. 28, pp. 267–340, 1974.
- [58] ——, "Theoretical formalism for the sliding filament model of contraction of striated muscle part ii," *Prog. Biophys. Mol. Biol.*, vol. 29, pp. 105–159, 1976.
- [59] C. Jia, R. Olafsson, K. Kim, T. J. Kolias, J. M. Rubin, W. F. Weitzel, R. S. Witte, S.-W. Huang, M. S. Richards, C. X. Deng et al., "Twodimensional strain imaging of controlled rabbit hearts," *Ultrasound Med. Biol.*, vol. 35, no. 9, pp. 1488–1501, 2009.
- [60] J. Bercoff, S. Chaffai, M. Tanter, L. Sandrin, S. Catheline, M. Fink, J. Gennisson, and M. Meunier, "In vivo breast tumor detection using transient elastography," *Ultrasound Med. Biol.*, vol. 29, no. 10, pp. 1387– 1396, 2003.
- [61] L. A. Chernak and D. G. Thelen, "Tendon motion and strain patterns evaluated with two-dimensional ultrasound elastography," *J. Biomech.*, vol. 45, no. 15, pp. 2618–2623, 2012.
- [62] M. A. Lubinski, S. Y. Emelianov, and M. O'Donnell, "Speckle tracking methods for ultrasonic elasticity imaging using short-time correlation,"

- IEEE Trans. Ultrason. Ferroelectr. Freq. Control, vol. 46, no. 1, pp. 82–96, 1999.
- [63] A. Manduca, T. E. Oliphant, M. A. Dresner, J. Mahowald, S. A. Kruse, E. Amromin, J. P. Felmlee, J. F. Greenleaf, and R. L. Ehman, "Magnetic resonance elastography: non-invasive mapping of tissue elasticity," *Med. Image Anal.*, vol. 5, no. 4, pp. 237–254, 2001.
- [64] A. R. Skovoroda, M. A. Lubinski, S. Y. Emelianov, and M. O'Donnell, "Nonlinear estimation of the lateral displacement using tissue incompressibility," *IEEE Trans. Ultrason. Ferroelectr. Freq. Control*, vol. 45, no. 2, pp. 491–503, 1998.
- [65] M. Debella-Gilo and A. Kääb, "Sub-pixel precision image matching for measuring surface displacements on mass movements using normalized cross-correlation," *Remote Sens. Environ.*, vol. 115, no. 1, pp. 130–142, 2011.
- [66] N. Sharma, N. A. Kirsch, N. A. Alibeji, and W. E. Dixon, "A non-linear control method to compensate for muscle fatigue during neuromuscular electrical stimulation," *Front. Robot. AI*, vol. 4, p. 68, 2017.
- [67] Z. Sheng, V. Molazadeh, and N. Sharma, "Hybrid dynamical system model and robust control of a hybrid neuroprosthesis under fatigue based switching," in *Proc. Amer. Control Conf.*, 2018, pp. 1446–1451.